# Performance-enhanced eco-friendly triboelectric nanogenerator via wettability manipulation of lignin

Hongseok Jo[1], Dogun Park[2], Minkyeong Joo[2], Daekyu Choi[2], Jisong Kang[3], Jeong-Myeong Ha[3], Kwang Ho Kim[3], Ki Hyun Kim[4], and Seongpil An[2]

[1] Sungkyunkwan University (SKKU), SKKU Advanced Institute of Nanotechnology (SAINT), Sungkyunkwan University (SKKU)
[2]Sungkyunkwan University
[3]Korea Institute of Science and Technology
[4]Sungkyunkwan University (SKKU), School of Pharmacy

June 12, 2023

**Abstract**

Eco-friendly and sustainable energy harvests that can alleviate concerns on the energy crisis and environmental pollution are in demand. Exploiting nature-derived biomaterials is imperative to develop these carbon-neutral energy harvesters. In this study, lignin/polycaprolactone nanofiber (NF)-based triboelectric nanogenerators (TENGs) are fabricated using an electrospinning technique. Nanotextured morphology of electrospun lignin/polycaprolactone NFs and wettability modification of lignin into hydrophilicity can significantly enhance electron transfer between tribopositive and tribonegative materials, resulting in the highest energy-harvesting efficiency in their class. The output voltage of the lignin-based TENG exceeds 95 V despite relatively low tapping force of 9 N and frequency of 9 Hz. Various mechanical and physicochemical characterizations, including scanning electron microscopy (SEM), nuclear magnetic resonance (NMR) spectroscopy, X-ray diffraction (XRD) analysis, Fourier transform infrared (FTIR) analysis, and atomic force microscopy (AFM), are performed, confirming the mechanical durability, biocompatibility, and industrial viability of lignin-based TENG developed here.

## Performance-enhanced eco-friendly triboelectric nanogenerator via wettability manipulation of lignin

**Hongseok Jo [a,1], Dogun Park[a,b,1], Minkyeong Joo [a,b,1], Daekyu Choi [a,b], Jisong Kang [c, d], Jeong-Myeong Ha [d,e], Ki Hyun Kim[f,*], Kwang Ho Kim [d,g,h,*], and Seongpil An [a,b,i,j,*]**

[a] SKKU Advanced Institute of Nanotechnology (SAINT), Sungkyunkwan University (SKKU), Suwon 16419, Republic of Korea

[b] Department of Nano Science and Technology, Sungkyunkwan University (SKKU), Suwon 16419, Republic of Korea

[c] Department of Chemical and Biological Engineering, Korea University, Seoul 02841, Republic of Korea

[d] Clean Energy Research Center, Korea Institute of Science and Technology, Seoul 02792, South Korea

[e] Division of Energy and Environment Technology, KIST School, University of Science and Technology, Seoul 02792, South Korea

[f] School of Pharmacy, Sungkyunkwan University (SKKU), Suwon 16419, Republic of Korea

[g] KIST-SKKU Carbon-Neutral Research Center, Sungkyunkwan University (SKKU), Suwon, 16419, Republic of Korea

[h] School of Chemical Engineering, Sungkyunkwan University (SKKU), Suwon, 16419, Republic of Korea

[i] Department of Nano Engineering, Sungkyunkwan University (SKKU), Suwon 16419, Republic of Korea

[j] Department of Semiconductor Convergence Engineering, Sungkyunkwan University (SKKU), Suwon 16419, Republic of Korea

**Abstract**

Eco-friendly and sustainable energy harvests that can alleviate concerns on the energy crisis and environmental pollution are in demand. Exploiting nature-derived biomaterials is imperative to develop these carbon-neutral energy harvesters. In this study, lignin/polycaprolactone nanofiber (NF)-based triboelectric nanogenerators (TENGs) are fabricated using an electrospinning technique. Nanotextured morphology of electrospun lignin/polycaprolactone NFs and wettability modification of lignin into hydrophilicity can significantly enhance electron transfer between tribopositive and tribonegative materials, resulting in the highest energy-harvesting efficiency in their class. The output voltage of the lignin-based TENG exceeds 95 V despite relatively low tapping force of 9 N and frequency of 9 Hz. Various mechanical and physicochemical characterizations, including scanning electron microscopy (SEM), nuclear magnetic resonance (NMR) spectroscopy, X-ray diffraction (XRD) analysis, Fourier transform infrared (FTIR) analysis, and atomic force microscopy (AFM), are performed, confirming the mechanical durability, biocompatibility, and industrial viability of lignin-based TENG developed here.

Keywords : eco-friendly triboelectric nanogenerator, energy-harvesting technology, lignin, wettability manipulation, electrospinning

**[1] Hongseok Jo, Dogun Park, and Minkyeong Joo contributed equally to this work.**

***Corresponding authors:** esan@skku.edu, kwanghokim@kist.re.kr, khkim83@skku.edu

## Introduction

The overdependence on fossil fuels has raised increasing concerns about the energy crisis and environmental pollution. There have been significant efforts to find green and sustainable resources that can address these issues as new energy sources and materials. Nature-derived biomaterials are increasingly being considered as alternatives to existing petroleum-based materials.[1] These carbon-neutral biomaterials derived from plants and animals possess advantages unattainable by petroleum-based materials. First, they are non-toxic and biocompatible, making them suitable for energy applications that require direct interaction with humans or nature. Next, they are abundant in nature and thus easy to access, which can reduce the reliance on existing limited resources. Third, the biodegradability of nature-derived biomaterials can mitigate waste accumulation and environmental pollution.

Lignin, the most dominant aromatic polymer in nature, is found in terrestrial biomasses in the range of 15 – 40% weight.[2] it provides structural support to plants, contributing to their biomechanical strength. Lignin also plays important roles in water conduction from roots to leaves, and often serves as a defense system against harmful microbial invasion and various environmental stimuli. A large amount of lignin is produced as a by-product in pulp and paper making industries. Considering its attractive physicochemical properties, including thermal stability, durability, redox activity, and antioxidant property, lignin is viewed as a promising alternative to petroleum-based materials.[3] In addition, lignin has unique structural and chemical features that make it an excellent building block for manufacturing functional materials for energy applications. For example, the aromatic backbone of lignin provides lignin-derived materials with high thermal stability and structural rigidity.[4]Furthermore, the aromatic rings form π–π conjugated system that can facilitate producing various kinds of precursors.[5]

Because of these features, lignin has gained significant interest as a carbon-neutral and sustainable biomaterial. In addition, the ease of incorporation of lignin into various existing manufacturing processes is also advantageous for the development of industrially viable and scalable energy materials and devices.[6] Therefore, recent research and development efforts are focused on harnessing the potential of lignin to contribute to advancing renewable energy technologies, including energy-harvesting technologies. The triboelectric nanogenerator (TENG) is a representative energy-harvesting technology that can transduce mechanical energy, such as motion or vibration, into electrical energy based on the triboelectric effect.[7-9] An *et al.* reported eco-friendly triboelectric nanogenerators (eco-TENGs) using lignin-based nanofibers (NFs) with a solution-blowing technique.[10] In their study, the lignin NF mat was employed as the tribopositive material, while a polyamide tape served as the tribonegative materials. Although they for the first time reported the lignin NF-based TENG, a low output voltage of $< 1$ V was observed at the energy-harvesting tests. Similarly, Wang *et al.* recently reported eco-TENGs composed of lignin-based electro spun NFs and a Teflon film.[11]They could achieve a high output voltage of $> 100$ V under a high applied force of 40 N and a frequency of 10 Hz.

As demonstrated in the aforementioned studies, the combination of lignin and NF techniques is increasingly being preferred in the energy-related fields. Because the NF fabrication techniques, such as electrospinning and solution blowing, are facile, industrially scalable.[12, 13], and most importantly, capable of exploiting bare lignin powder directly without additional thermal or physicochemical treatments during their fabrication process. In addition, the nanotextured surface morphology of NF mat (or film) can maximize the effective friction area regardless of its projected contact surface area, thus can significantly increase the effect of contact electrification (or triboelectricity).[14] In this study, kraft lignin, wettability-manipulated hydrophilic, and hydrophobic lignins were prepared and electrospun, and then their energy-harvesting performance as tribopositive materials were explored (**Figure 1** ). More sophisticated electrospinning techniques and the use of the utmost tribonegative material, Teflon film, allowed the bare kraft lignin to yield a higher output voltage of $> 25$ V compared to the values observed from the work of An *et al* . despite similar test conditions.[10] Moreover, the wettability manipulation of kraft lignin to hydrophilicity could enhance its surface energy, thus leading to a remarkable increase in the output voltage value over 90 V even with a lower applied force of 9 N than that of the work of Wang *et al.* [11] Accordingly, the utilization of lignin, the second most abundant biomaterial among natural biomaterials, combined with surface wettability design methods demonstrated here, holds significant promise as an industrially viable and sustainable energy material and technique.

## 2. Results and discussion

### 2.1. Fabrication of lignin/polycaprolactone nanofiber-based triboelectric nanogenerator

Lignin, a major component of lignocellulosic biomass, was employed to fabricate biodegradable and sustainable nanofiber (NF) mats via electrospinning. The structure of lignin was modified to improve its processability. The electrospinning process is commonly employed to produce nonwoven NF mats. However, electrospinning with low molecular weight ($M_{\mathrm{w}}$) lignin is challenging due to its insufficient viscoelasticity, which is essential for self-sustainable electrospinning (**Table 1** ).[15-17] Therefore, polycaprolactone (PCL), which has a relatively high molecular weight ($M_{\mathrm{w}}$) of 80,000 kDa and thus can enhance the electrospinnability of lignin, was incorporated with lignin. To evaluate the influence of lignin wettability on its energy-harvesting performance (cf. **Section 2.3** ), we prepared a bare PCL solution and three kinds of different lignin/PCL solutions. For lignin/PCL solutions, a lignin/PCL ratio was the same as 1:1 (w/w) while lignins with different wettabilities were used. The three variants of lignins, namely kraft, hydrophilic, and hydrophobic lignins, were prepared, then mixed with PCL before electrospinning (cf. **Sections S1.2** and **S1.3** ). Henceforth, these different lignin/PCL combinations are denoted as KLP, HILP, and HOLP, respectively.

The fabrication of lignin/PCL NF-based triboelectric nanogenerators (LP-TENGs) involves several steps. First, electrospun LP NF mats (*i.e.* , KLP, HILP, and PCL NF mats) and tribonegative Teflon tape were transferred to a Cu substrate that served as the electrode. Second, they were affixed to a polyvinyl chloride (PVC) film, which provided structural support and resistance to pressure (**Figure S1a** ). The illustration at the bottom of **Figure 1** demonstrates the operation mechanism of the LP-TENG, which relies on the contact-induced triboelectric effect. Although the exact underlying principles of the triboelectric effect

remain unclear, it is widely recognized that this phenomenon arises from electron transfers occurring at the interface of dissimilar materials owing to the overlapping of the electron clouds of different atoms (or molecules).[18] When materials exhibiting distinct electrical polarization come into contact or separate from each other under the influence of external forces, the interaction at the interface induces friction, resulting in the generation of positive and negative charges on their respective surfaces. This charge imbalance establishes a potential difference between the materials, thereby facilitating the movement of electrons through an external circuit.[19]

2.2. Mechanical properties of lignin/polycaprolactone nanofibers

Photos and scanning electron microscopy (SEM) images of the KLP, HILP, and HOLP NF mats are shown in**Figure 2**. Lignins, the main component of LP-TNEGs, retained their inherent coloration, and these colors revealed their identities when the lignins were combined with PCL **(Figure S1b)**. The introduction of different lignins into the PCL resulted in a noticeable reduction in the brown color of the resulting NF mats (**Figures 2a**, **2b**, and **2c**). The degree of color change in the lignin/PCL NF mats was found to be correlated with the specific lignin powder employed, with KL, HIL, and HOL powders resulting in a lighter shade in order. In addition, discernible changes were observed in the morphology and mechanical properties of the lignin/PCL NF mats. The average diameter ($D_{\mathrm{avg}}$) of the lignin/PCL NF varied depending on the wettability of lignin, despite using a constant lignin/PCL ratio and the same electrospinning conditions. Compared to the pristine PCL NFs with $D_{\mathrm{avg}}$ =103 nm (**Figures S2a** and **Sb**), the lignin/PCL NFs showed an increase in $D_{\mathrm{avg}}$ for all lignin cases. Among the different lignin/PCL NF cases, the HOLP NFs exhibited a smaller$D_{\mathrm{avg}}$ of 136 nm than those of KLP and HIL NFs, which had $D_{\mathrm{avg}}$ of 218 and 273 nm, respectively (**Figure 2d**).

The wettability manipulation of lignin also had a significant influence on the mechanical properties of the resulting lignin/PCL NF mats.**Figure 2e** presents the results of the tensile tests conducted on the KLP, HILP, and HOLP NF mats. The values of Young's modulus ($E$ ) and yield strength ($Y$ ) were obtained by using the elastic–plastic Green equation [$\sigma = Y\tanh(E\epsilon\ /\ Y$ ), where $\sigma$ and $\epsilon$ are the tensile stress and strain measured experimentally].[20] The values of $E$ and $Y$ for the pristine PCL NF mat were 6.16 ± 0.02 and 0.05 ± 0.02 MPa, respectively (**Figure S2c** ). The incorporation of KL, HIL, and HOL into PCL led to improvement in mechanical properties. The HILP NF mat exhibited the highest $E$value of 15.95 ± 4.32 MPa among all the NF mats, which is seemingly attributed to its highest value in $D$ . On the other hand, the$Y$ values of the KLP, HILP, and HOLP NF mats were 2.66 ± 0.69, 2.93 ± 0.57, and 7.31 ± 0.12 MPa, respectively, which shows that blending higher $M_{\mathrm{w}}$ lignins into PCL resulted in higher $Y$ values (**Table 1** and **Figure 2e** ). The higher $M_{\mathrm{w}}$ lignins possess longer polymeric chains, which can enhance intermolecular interactions and entanglement inside of individual NFs.[21, 22] Thus, these enhanced intermolecular behaviors improved the mechanical strength of the NF mats.

2.3. Physicochemical properties of lignin/polycaprolactone nanofibers

To examine molecular structures, presence of ordered domains, and chemical features of KL, HIL, and HOL, their powders were investigated using $^1$H nuclear magnetic resonance (NMR) spectroscopy, X-ray diffraction (XRD), and Fourier transform infrared (FTIR) spectroscopy. **Figure 3a** shows the $^1$H NMR spectra observed from KL, HIL, and HOL powders. The characteristic peaks of KL observed at $\delta = 2.57$, 3.41, and 3.87 ppm are attributed the protons of methylene and methoxy groups,[23-27] and the broad peak between $\delta = 6.79$ and 6.97 ppm represents the proton of the phenyl ring in KL.[26, 28, 29] With the chemical treatment of KL to HIL, the new peak was detected at $\delta = 3.14$ ppm, which corresponds to the proton of methanimine group with N-$CH_3$bond.[30, 31] In the spectra of HIL, the characteristics peaks associated with KL were found at $\delta = 3.87$ and 6.79 to 6.97 ppm, indicating that the lignin backbone structure retained even after chemical modification. In addition, the prominent peak observed at$\delta = 4.70$ ppm is attributed to the absorption of $H_2O$, thereby indicating that the hydrophilic surface exhibits the capability to adsorb water molecules in air through the formation of hydrogen bonds with hydroxyl groups in HIL.[32-34]

Upon subjecting KL to hydrophobic chemical treatment, the characteristic peaks of KL were found at $\delta$

= 2.57, 3.84, and 6.79 to 6.97 ppm, confirming the preservation of the macromolecular lignin backbone. Furthermore, the resulting NMR spectrum of HOL revealed characteristic peaks associated with palmitic groups. The peaks corresponding to different functional groups within the palmitic structure, namely $CH_3$ (methyl), aliphatic $CH_2$ (methylene), -$CH_2$-$CH_2$-C(=O)-, and -$CH_2$-(C=O)-, were observed at $\delta = 0.91$, 1.27, 1.63–1.77, and 7.26 ppm, respectively.[35, 36] The emergence of these new peaks, specifically those associated with the methyl ($CH_3$) and methylene ($CH_2$) groups, can be attributed to the increased hydrophobicity of HOL.[37, 38]

Chemical distinctions between KL, HIL, and HOL were also identified in the FTIR spectra (**Figure S3a** ). The FTIR band assignment obtained from KL were presented in **Table S1** .[11, 39-42] Chemical modification of KL induced a change in the chemical structures of both HIL and HOL. In the FTIR spectrum of HIL, the weak signal of band at 1708 $cm^{-1}$, which is observed in the KL spectrum, indicated the presence of unconjugated carbonyl groups after KL modification.[43]On the other hand, in the FTIR spectrum of HOL, the absence of broad band from 3600 to 3000 $cm^{-1}$ was attributed to substitute palmitic groups ($C_{15}H_{31}$) for O–H group. The prominent emergence of band at 2915 $cm^{-1}$ and strong signal of band at 2848 $cm^{-1}$ in the HOL spectrum, corresponding to the asymmetric and symmetric C–H stretching vibrations of aliphatic methylene (–$CH_2$–),[44-46] signify the transformation of kraft lignin into hydrophobic lignin. Furthermore, the strong signal of band at 1708 $cm^{-1}$ was ascribed to the presence of C=O bond as substituting palmitic groups ($C_{15}H_{31}$) for O–H group.

The XRD patterns revealed significant variations in the phase characteristics of lignin due to hydrophilic and hydrophobic treatments. As presented in **Figure S3b** , two broad peaks corresponding to the ordered domain and amorphous region of biomass were observed in the XRD spectra of KL at $2\vartheta = 22.2°$ and 40°, respectively.[44] With the functionalization of KL to HIL, the position of the peak associated with the ordered domain of lignin shifted from its original position at $2\vartheta = 22.2°$ to a lower angle of $2\vartheta = 19.1°$. This shift was attributed to the presence of a uniformly tensioned ordered domain within the lignin structure, achieved through the attachment of trimethylamine groups to the lignin framework.[47, 48] However, the XRD pattern of HOL exhibited significant changes compared to those of KL and HIL. These changes were attributed to the incorporation of the palmitic group in the KL molecule. The peaks observed in the XRD pattern of HOL at $2\vartheta = 21.3°$ and 23.9° were identified as the presence of fatty acid crystals corresponding to the palmitic groups.[49, 50] In addition, the HOL peak associated with the ordered domain of lignin shifted toward $2\vartheta = 20.3°$ owing to the uniform tensile stress exerted on the ordered domain. This resulted in the attachment of the palmitic groups onto the lignin framework.

The $M_w$ of KL, HIL, and HOL were determined using gel permeation chromatography (GPC). An alternative approach combining elemental analysis and degree of substitution was employed to analyze the $M_w$ of HIL, which was insoluble in the GPC mobile phase. The results presented in **Table 1** reveal that KL, HIL, and HOL had $M_w$ values of 4.826, 6.654, and 13.430 g $mol^{-1}$, respectively. In comparison to$M_w$ of KL, the mass percentages of HIL and HOL significantly increased by 37.8% and 178.3%, respectively, which was attributed to the presence of functional groups in HIL and HOL.

The physicochemical difference depending on lignins was also evident in the lignin/PCL NF mats. **Figures 3b** and **3c** present the FTIR spectra and XRD patterns of the pristine PCL, KLP, HILP, and HOPL NF mats. The FTIR spectra of all NF mats exhibited the characteristic bands of the PCL NF mat at 2947, 2866, and 1720 $cm^{-1}$, corresponding to asymmetric elongation of the methylene-oxygen ($CH_2$-O), symmetric methylene groups ($CH_2$-), and vibration of –C=O bonds, respectively.[51, 52] This indicates the presence of PCL within all NF mats. The FTIR spectra of the KLP and HILP NF mats revealed the same bands observed from KL and HIL powders; O–H stretching (3600˜3000 $cm^{-1}$) and aromatic C=C (1600 and 1515 $cm^{-1}$). However, discernible changes in the FTIR spectrum of the HOLP NF mats were observed, *i.e.* , the elimination and the reduction of the characteristic bands of O–H and aromatic C=C. Meanwhile, new bands of C–H bonds (2915 and 2848 $cm^{-1}$) and C=O ester (1708 $cm^{-1}$), which are related to the hydrophobic feature and observed from HOL powder, were also observed in the FTIR spectrum of HOLP NF mat (**Figure 3b** ).

Contrary to the analyses above, no discernible difference between the NF mats was observed in the XRD

result (**Figure 3c** ). For the pristine PCL NF mat, the XRD pattern exhibited two intense peaks at $2\vartheta =$ 21.4° and 23.6°, indicative of the (110) and (200) PCL lattice phases, respectively.[53] A broad peak in the range of 10–20° attributed to the semicrystalline phase was also observed. The dominant (110) and (200) lattice planes in the PCL NF mat were also observed in both the KLP and HILP NF mats. In case of the HOLP NF mat, a peak at $2\vartheta = 23.9°$, which corresponds to the presence of fatty acid crystal, was also found.

The thermal stability and degradation behavior of the HILP and HOLP NF mats, compared to the KLP NF mat, were evaluated through thermogravimetric analysis (TGA). **Figure 3d** shows the TG curves of the specimens. The thermal degradation process of the HILP NF mat was observed to occur in four stages, whereas that of the KLP and HOLP NF mats occurred in two stages. The two thermal degradations observed in the KLP and HOLP NF mats correspond to the decomposition of phenolic groups in the lignin (150–320 degC) and the decomposition of PCL and lignin (320–500 degC), respectively.[54, 55] A significant decomposition occurred around 250 degC of the HOLP NF mat is attributed to the thermal degradation of palmitic groups. The first thermal degradation of the HILP NF mat between 30 and 100 degC, presenting a weight loss of 2%, resulted from the loss of water initially absorbed from ambient moisture because of the hydrophilicity of HILP. This result agrees well with the $^1$H NMR and FTIR analyses. The second degradation occurred between 130 and 300 degC, corresponding to a weight loss of 12%, is attributed to the decomposition of the cationic group substituted from the hydroxyl group in KL. The third degradation observed between 300 and 350 degC ascribed to the cleavage of inter-unit linkages of lignin.[56, 57] The fourth degradation between 350 and 500 degC corresponds to the comprehensive decomposition of PCL and lignin.

The modified functional groups in HIL and HOL resulted in changes in the wettability of the corresponding NF mats (**Figure 3e** ). The water contact angle (WCA) of the PCL NF mat was 134deg, predominantly because of the hydrophobic properties of the C–H bonds in the methylene group. The introduction of KL into PCL led to a reduction in WCA to 108deg. The hydrophilic O–H groups from KL is responsible for this wettability change. The HILP NF mat, where the C–H bonds of the methylene and methoxy groups were eliminated through the chemical treatment, exhibited a significant further decrease in WCA to 28deg. The HOLP NF mat showed the highest WCA of 138deg. The additional C–H bonds present in HOLP contributed to its enhancement in hydrophobic nature.

The modified functional groups resulting from the chemical treatment of KL to HIL and HOL conversely influenced the electrostatic potential states of the resulting NF mats. This was evaluated through surface potential ($\varphi$ ) measurements (**Figure 3f** ). For HILP NF mat,$\varphi$ was measured to be 248 mV, indicating the presence of a positive charge on its surface. The positive charge is attributed to the cationic site of the quaternary ammonium substituents ($-N^+(CH_3)_3$) introduced during the modification process to transform KL into HIL.[58, 59] On the other hand, the HOLP NF mat exhibited $\varphi$ of 82 mV, implying the degree of negative surface charge is higher than the HILP NF mat. This is due to the protonation of the carboxyl group in HOLP.[59, 60] The presence of positive or negative surface charges can affect the charge transfer and accumulation during the triboelectric process. Indeed, the chemical treatments of KL to HIL and HOL significantly impacted the energy-harvesting performance of the resulting NF mats, which is further discussed in the forthcoming section.

### 2.4. Energy-harvesting performance of lignin/polycaprolactone nanofiber-based triboelectric nanogenerator

**Figures 4a–4d** present the output voltage ( $V$ ) signals of the LP-TENGs composed of the KLP, HILP, and HOLP NF mats under different tapping conditions of applied force ( $F$ ) and frequency ( $f$ ). Teflon tape was selected as the tribonegative material because of its low surface energy. The KLP- and HILP-TENGs exhibited increases in $V$ signals with increasing $F$ (**Figures 4a** and**4b** ). On the other hand, no discernible effect on $V$ signals was observed for the HOLP-TENG. The maximum output positive voltage ( $V_{max}$) of the HILP-TENG increased from 22 to 60 V and further to 96 V as the $F$ increased from 3 to 6 and 9 N, respectively. However, those of the HOLP-TENG were just 12, 16, and 15 V when the $F$ were 3, 6, and 9 N, respectively. Similarly, the $V$ signals of all LP-TENGs increased as the $f$ increased from 3 to 9 Hz (**Figures 4c** and **4d** ). This is because of a decrease in contact time ( $t$ ), corresponding to an increase in the tapping speed, thus leading to an increase in $V$ ($= RI = Rq/t$ , where $R$ is an external load and $q$ is

the surface charge).[61] Note that this behavior can be explained because the LP-TENGs were evaluated at the short-circuit condition.

The superior energy-harvesting performance of the HILP-TENG was attributed to an increase in electron exchange between tribo-positive and -negative materials because of the increased distinction in their electrostatic potential. When tribo-positive and -negative materials with different electrostatic potential come into contact, electrons are hopped from the high-electrostatic-potential material to the low-electrostatic-potential one.[8, 62] Because of the electron transfer, a potential difference between two dissimilar materials is generated. The higher surface electrostatic potential of tribopositive HILP NF mat led to a further increase in the surface electrostatic potential difference against the tribonegative Teflon film, thus resulting in a greater potential difference, thereby exhibiting higher $V$ signals.

Cyclic tests by repetitive tapping on the KLP-, HILP-, and HOLP-TENGs were conducted (**Figure 4e** ). 100,000 tapping cycles were performed with fixed $F$ of 9 N and $f$ of 9 Hz. The KLP-TENG exhibited a slight increase in $V_{max}$ from $V$= ˜ 15 to ˜ 30 V during the test while the HILP-TENG showed a significant increase in $V_{max}$ from $V$ = ˜ 30 to ˜ 80 V (**Figure S4a** ). This gradual increase in $V$ over hundreds of thousands of cycles originates from the unique morphological structure of the nonwoven NF mat, as discussed in other previously-reported studies.[63] The NFs are continuously compressed during the repetitive tapping, which contributes to an increase in the actual contact area between NFs, thus facilitating the gradual rise in $V$.

The energy-harvesting efficiency $\eta$ , defined as $\eta = V_{max} F^{-1} S^{-1}$, where $S$ is the projected contact surface area,[10] of the HILP-TENGs and previously-reported tribopositive biopolymer-based TENGs are compared in**Figure 4f** and **Table 2** . Note that other tribopositive biopolymer-based TENGs that did not provide specific $V_{max}$,$F$ , or $S$ values are not described here. The HILP-TENG in this study exhibited an outstanding $\eta$ value of 4133.33 V $N^{-1}$ $m^{-2}$ despite a relatively small$S$ (see the red star in **Figure 4f** ), demonstrating its great potential as an eco-friendly and sustainable high performance energy harvester.

**Figure 5** shows the industrial potential of HILP-TENG as a kinetic energy harvester. The output performance of the HILP-TENG was evaluated by exploring the variations in the peak-to-peak voltage ( $V_{ptop}$) and current ($I_{ptop}$) as varying the external load ($R$ ) from $10^5$ to $10^9$ Ω (**Figures 5a** and **5b** ). Repetitive tapping was conducted under tapping conditions of $F$ = 9 N and $f$ = 9 Hz. As the $R$increased, the $V_{ptop}$ increased up to 75 V while the $I_{ptop}$ decreased to 0.3 μA, which aligns with the principles outlined in Ohm's law. The resultant maximum output power ($P$ ) and output power density ($PS^{-1}$) at$R$ = $2\times10^7$ Ω, were 392 μW and 157 mW $m^{-2}$, respectively.

**Figures 5c** and **S4b** depict the current ($I$ ) signals obtained from HILP- and HOLP-TENGs under tapping conditions of$F$ = 9 N and $f$ = 9 Hz, allowing to quantify of the surface charge accumulation occurring in the HILP- and HOLP-TENGs. For the HILP-TENG, the magnitudes of the positive and negative surface charges during a single tapping ($q_{pos}$ and$q_{neg}$, respectively) were almost the same with showing $q_{pos}$ = $2.42\times10^{-8}$ C and$q_{neg}$ = $-2.42\times10^{-8}$ C. The similarity in the magnitudes of $q_{pos}$ and$q_{neg}$ indicates that the electrons engaged in the pressing motion were equally involved in the subsequent release motion during repetitive tapping of the HILP-TENG. For the HOLP-TENG, it exhibited lower magnitudes in both $q_{pos}$ and$q_{neg}$ values measured to be $1.93\times10^{-8}$ and $1.92\times10^{-8}$ C, respectively.

To further investigate the effect of the surface charge of HILP and HOLP on the surface potential distribution of the different triboelectric pairs, we also performed COMSOL Multiphysics simulations (**Figure 5d** ). The surface charge density ($\sigma_0$) was calculated as:

, (1)

where $q$ and $S$ are the charge resulting from the accumulation of current (**Figures 5c** and **S4b** ) and the size of the TENG, respectively. The transferred charge density ($\sigma$ ') upon the contact of the tribo-positive and -negative materials can be expressed as a function of $\sigma_0$as:[64]

, (2)

where $d_{\text{gap}}$, $d_{\text{PTFE}}$, and $\epsilon_{\text{PTFE}}$ are the gap distance, thickness, and dielectric constant of the PTFE (Teflon) film, respectively. Then, the electric potential ($V_{\text{p}}$) generated by the TENG can be obtained as:

, (3)

where $\epsilon$ is the vacuum permittivity ($8.85 \times 10^{-12}$ F m$^{-1}$). As presented in **Eq. (3)** , $V_{\text{p}}$ is proportional to $q$ . Based on the results obtained from COMSOL with the presented parameters (**Table S2** ), it can be predicted that the HILP-TENGs demonstrate a higher potential difference between the top and bottom layers than the HOLP-TENGs, which agrees well with the experimental results.

The utilization of a full-wave bridge rectifier circuit along with capacitors enabled the accumulation of output voltage (**Figure 5e** ). Given tapping conditions of $F = 9$ N and $f = 9$ Hz, the electrical energy could be effectively stored in various capacitors having capacitances of 0.22, 2 and 22 μF. The 0.22, 2, and 22 μF capacitors were charged to 0.28, 0.25 and 0.01 V, respectively. The HILP-TENGs also demonstrated the capability of running 34 individual LEDs by repetitive tapping (**Figure 5F** and **Movie S1** ), showing the potential of the HILP-TENG for self-powered electronic devices.

To demonstrate the development of TENGs without petroleum-based materials, we also fabricated the HILP-HOLP-TENG. In contrast to the HILP-TENG, the HILP-HOLP-TENG employed the HOLP NF mat as a tribonegative material instead of using Teflon film (cf. **Figures 1** and **S1a** ). Then, its energy-harvesting performance was evaluated (**Figures S4c** , **5G** , and **Movie S2** ). For the cyclic tapping test with tapping conditions of $F = 9$ N and $f = 9$ Hz, the $V_{\text{max}}$ gradually increased from 15 to 35 V (**Figure S4c** ), showing a reasonable energy-harvesting performance even without using Teflon film. Furthermore, we also demonstrated that when a user engages in activities such as walking or running, the HIILP-HOLP-TENG can produce $V$ signals. This remarkable capability of the HIILP-HOLP-TENG demonstrates their potential for practical energy generation from everyday human motion.

## 3. Conclusions

Kraft, hydrophilic, and hydrophobic lignins were prepared, followed by an electrospinning process. The electrospun nonwoven kraft, hydrophilic, and hydrophobic lignin nanofibers (NFs) were evaluated as tribopositive materials of triboelectric nanogenerators (TENGs). The enhancement in the surface energy of hydrophilic lignin NFs enabled the TENG to exhibit an outstanding output voltage over 95 V at a tapping force and frequency of 9 N and 9 Hz, respectively. The energy-harvesting efficiency, which considered the output voltage with the size and applied tapping conditions of the tested TENG, was 4133 V N$^{-1}$m$^{-1}$, showing the highest value among the other previously-reported biomaterial-based TENGs. Furthermore, a TENG entirely based on both tribo-positive and -negative lignin NFs was demonstrated, which also exhibited a reasonable energy-harvesting performance at user-engaged activities, such as walking and running.

## Acknowledgements

This work was partly supported by a National Research Foundation of Korea (NRF) grant funded by the Korea Government (MSIT) RS-2023-00211303, Korea Institute for Advancement of Technology (KIAT) grant funded by the Korea Government (MOTIE) (P0023521, HRD Program for Industrial Innovation), and the Postdoctoral Research Program of Sungkyunkwan University (2023)

## References

1. K.Y. Song, S.W. Kim, D.C. Nguyen, J.Y. Park, T.T. Luu, D. Choi, J.M. Baik, S. An. Recent progress on nature-derived biomaterials for eco-friendly triboelectric nanogenerators. *EcoMat*. 2023:e12357. doi:*https://doi.org/10.1002/eom2.12357*2. A.J. Ragauskas, G.T. Beckham, M.J. Biddy, R. Chandra, F. Chen, M.F. Davis, B.H. Davison, R.A. Dixon, P. Gilna, M. Keller. Lignin valorization: improving lignin processing in the biorefinery.*Science*. 2014;344(6185):1246843. doi:*https://doi.org/10.1126/science.1246843*3. D. Wang, S.H. Lee, J. Kim, C.B. Park. "Waste to wealth": lignin as a renewable building block for energy harvesting/storage and environmental remediation. *ChemSusChem*. 2020;13(11):2807-2827. doi:*https://doi.org/10.1002/cssc.202000394*4. W.-J. Chen, C.-X. Zhao, B.-Q. Li, T.-Q. Yuan, Q. Zhang.

Lignin-derived materials and their applications in rechargeable batteries. *Green Chem.* 2022;24(2):565-584. doi:*https://doi.org/10.1039/D1GC02872C*5. D. Kai, M.J. Tan, P.L. Chee, Y.K. Chua, Y.L. Yap, X.J. Loh. Towards lignin-based functional materials in a sustainable world. *Green Chem.* 2016;18(5):1175-1200. doi:*https://doi.org/10.1039/C5GC02616D*6. W. Qu, J. Yang, X. Sun, X. Bai, H. Jin, M. Zhang. Towards producing high-quality lignin-based carbon fibers: A review of crucial factors affecting lignin properties and conversion techniques. *Int. J. Biol. Macromol.* 2021;189:768-784. doi:*https://doi.org/10.1016/j.ijbiomac.2021.08.187*7. G. Zhu, B. Peng, J. Chen, Q. Jing, Z.L. Wang. Triboelectric nanogenerators as a new energy technology: From fundamentals, devices, to applications. *Nano Energy.* 2015;14:126-138. doi:*https://doi.org/10.1016/j.nanoen.2014.11.050*8. C. Wu, A.C. Wang, W. Ding, H. Guo, Z.L. Wang. Triboelectric nanogenerator: a foundation of the energy for the new era. *Adv. Energy Mater.* 2019;9(1):1802906. doi:*https://doi.org/10.1002/aenm.201802906*9. S.A. Lone, K.C. Lim, K. Kaswan, S. Chatterjee, K.-P. Fan, D. Choi, S. Lee, H. Zhang, J. Cheng, Z.-H. Lin. Recent advancements for improving the performance of triboelectric nanogenerator devices. *Nano Energy.* 2022:107318. doi:*https://doi.org/10.1016/j.nanoen.2022.107318*

10. S. An, A. Sankaran, A.L. Yarin. Natural biopolymer-based triboelectric nanogenerators via fast, facile, scalable solution blowing. *ACS Appl. Mater. Interfaces* . 2018;10(43):37749-37759. doi:*https://doi.org/10.1021/acsami.8b15597*

11. J. Wang, Y. Chen, Y. Xu, J. Mu, J. Li, S. Nie, S. Chen, F. Xu. Sustainable lignin-based electrospun nanofibers for enhanced triboelectric nanogenerators. *Sustainable Energy Fuels* . 2022;6(8):1974-1982. doi:*https://doi.org/10.1039/D1SE02005F*

12. A. Kolbasov, S. Sinha-Ray, A. Joijode, M.A. Hassan, D. Brown, B. Maze, B. Pourdeyhimi, A.L. Yarin. Industrial-scale solution blowing of soy protein nanofibers. *Ind. Eng. Chem. Res.* 2016;55(1):323-333. doi:*https://doi.org/10.1021/acsami.8b15597*

13. Y. Huang, J. Song, C. Yang, Y. Long, H. Wu. Scalable manufacturing and applications of nanofibers. *Mater. Today* . 2019;28:98-113.doi:*https://doi.org/10.1016/j.mattod.2019.04.018*

14. J. Chen, Y. Huang, N. Zhang, H. Zou, R. Liu, C. Tao, X. Fan, Z.L. Wang. Micro-cable structured textile for simultaneously harvesting solar and mechanical energy. *Nat. Energy* . 2016;1(10):1-8. doi:*https://doi.org/10.1038/nenergy2016138*

15. B.L. Dargaville, C. Vaquette, F. Rasoul, J.J. Cooper-White, J.H. Campbell, A.K. Whittaker. Electrospinning and crosslinking of low-molecular-weight poly (trimethylene carbonate-co-l-lactide) as an elastomeric scaffold for vascular engineering. *Acta Biomater* . 2013;9(6):6885-6897. doi:*https://doi.org/10.1016/j.actbio.2013.02.009*

16. A.L. Yarin, B. Pourdeyhimi, S. Ramakrishna, Fundamentals and applications of micro-and nanofibers, Cambridge University Press, Cambridge, 2014.

17. X. Wang, C. Pellerin, C.G. Bazuin. Enhancing the electrospinnability of low molecular weight polymers using small effective cross-linkers.*Macromolecules* . 2016;49(3):891-899. doi:*https://doi.org/10.1021/acs.macromol.5b02670*

18. C. Xu, Y. Zi, A.C. Wang, H. Zou, Y. Dai, X. He, P. Wang, Y.C. Wang, P. Feng, D. Li. On the electron-transfer mechanism in the contact-electrification effect. *Adv. Mater.* 2018;30(15):1706790. doi:*https://doi.org/10.1002/adma.201706790*

19. S. Pan, Z. Zhang. Triboelectric effect: A new perspective on electron transfer process. *J. Appl. Phys* . 2017;122(14):144302. doi:*https://doi.org/10.1063/1.5006634*

20. A.E. Green. Hypo-elasticity and plasticity. *Proc. R. Soc. London, Ser. A* . 1956;234(1196):46-59. doi:*https://doi.org/10.1098/rspa.1956.0014*

21. Y. Termonia, P. Meakin, P. Smith. Theoretical study of the influence of the molecular

weight on the maximum tensile strength of polymer fibers. *Macromolecules* . 1985;18(11):2246-2252. doi:*https://doi.org/10.1021/ma00153a032*

22. T. Fornes, P. Yoon, H. Keskkula, D. Paul. Nylon 6 nanocomposites: the effect of matrix molecular weight. *Polymer* . 2001;42(25):09929-09940. doi:*https://doi.org/10.1016/S0032-3861(01)00552-3*

23. K. Lundquist. NMR studies of lignins. 5. Investigation of non-derivatized spruce and birch lignin by $^1$HNMR spectroscopy. *Acta Chem. Scand. B* . 1981;35:497-501. doi:*https://doi.org/10.3891/acta.chem.scand.35b-0497*

24. Z. Strassberger, S. Tanase, G. Rothenberg. The pros and cons of lignin valorisation in an integrated biorefinery. *RSC Adv.*2014;4(48):25310-25318. doi:*https://doi.org/10.1039/C4RA04747H*

25. D. Kai, K. Zhang, L. Jiang, H.Z. Wong, Z. Li, Z. Zhang, X.J. Loh. Sustainable and antioxidant lignin–polyester copolymers and nanofibers for potential healthcare applications. *ACS Sustainable Chem. Eng.*2017;5(7):6016-6025. doi:*https://doi.org/10.1021/acssuschemeng.7b00850*

26. I.V. Pylypchuk, P.r.A. Linden, M.E. Lindstrom, O. Sevastyanova. New insight into the surface structure of lignin nanoparticles revealed by$^1$H liquid-state NMR spectroscopy. *ACS Sustainable Chem. Eng.* 2020;8(36):13805-13812. doi:*https://doi.org/10.1021/acssuschemeng.0c05119*

27. A. Adjaoud, R. Dieden, P. Verge. Sustainable esterification of a soda lignin with phloretic acid. *Polymers* . 2021;13(4):637. doi:*https://doi.org/10.3390/polym13040637*

28. D. Kai, W. Ren, L. Tian, P.L. Chee, Y. Liu, S. Ramakrishna, X.J. Loh. Engineering poly (lactide)–lignin nanofibers with antioxidant activity for biomedical application. *ACS Sustainable Chem. Eng.*2016;4(10):5268-5276. doi:*https://doi.org/10.1021/acssuschemeng.6b00478*

29. H.V. Halleraker, T. Barth. Quantitative NMR analysis of the aqueous phase from hydrothermal liquefaction of lignin. *J. Anal. Appl. Pyrolysis* . 2020;151:104919. doi:*https://doi.org/10.1016/j.jaap.2020.104919*

30. B.C. Percival, M. Grootveld, M. Gibson, Y. Osman, M. Molinari, F. Jafari, T. Sahota, M. Martin, F. Casanova, M.L. Mather. Low-field, benchtop NMR spectroscopy as a potential tool for point-of-care diagnostics of metabolic conditions: Validation, protocols and computational models. *High-Throughput* . 2018;8(1):2. doi:*https://doi.org/10.3390/ht8010002*

31. B.-H. Han. Chemical structure analysis of non-ionic monomer contrast agents using $^1$H-NMR spectroscopy. *J. Radiol. Sci. Technol.* 2021;44(4):335-342. doi:*https://doi.org/10.17946/JRST.2021.44.4.335*

32. R. Wahlström, A. Kalliola, J. Heikkinen, H. Kyllönen, T. Tamminen. Lignin cationization with glycidyltrimethylammonium chloride aiming at water purification applications. *Ind. Crops Prod.*2017;104:188-194. doi:*https://doi.org/10.1016/j.indcrop.2017.04.026*

33. L. Chen, X. He, H. Liu, L. Qian, S.H. Kim. Water adsorption on hydrophilic and hydrophobic surfaces of silicon. *J. Phys. Chem. C* . 2018;122(21):11385-11391. doi:*https://doi.org/10.1021/acs.jpcc.8b01821*

34. O. Gordobil, R. Herrera, F. Poohphajai, J. Sandak, A. Sandak. Impact of drying process on kraft lignin: lignin-water interaction mechanism study by 2D NIR correlation spectroscopy. *J. Mater. Res. Technol.*2021;12:159-169. doi:*https://doi.org/10.1016/j.jmrt.2021.02.080*

35. J.V. Barbosa, F. Oliveira, J. Moniz, F.D. Magalhães, M.M. Bastos. Synthesis and characterization of allyl fatty acid derivatives as reactive coalescing agents for latexes. *J. Am. Oil Chem. Soc.*2012;89:2215-2226. doi:*https://doi.org/10.1007/s11746-012-2114-y*

36. A.K. Mishra, J.N. Moorthy. Mechanochemical catalytic oxidations in the solid state with in situ-generated Modified IBX from 3, 5-di-tert-Butyl-2-iodobenzoic acid (DTB-IA)/oxone. *Org. Chem. Front.* 2017;4(3):343-349. doi:*https://doi.org/10.1039/C6QO00588H*

37. T. Matsumoto, E. Kannan, M. Tomioka, T. Nishino. Effects of the high side-chain densities of hydrophobic poly (substituted methylene) s on their surface free energies. *Polym. J.* 2022;54(9):1081-1089. doi:*https://doi.org/10.1038/s41428-022-00656-6*

38. H. Zhu, Y. Liu, M. Zhu, H. Tang, J. Lin, D. Gu, J. Hao. Flexibility, size and hydrophobicity of alkyl side groups in methoxy-poly (ethylene glycol)-polypeptide for the nano-assembly and thermo-sensitivity.*Polymer* . 2022;263:125499. doi:*https://doi.org/10.1016/j.polymer.2022.125499*

39. H.L. Hergert. Infrared spectra of lignin and related compounds. II. Conifer lignin and model compounds1, 2. *J. Org. Chem.*1960;25(3):405-413. doi:*https://doi.org/10.1021/jo01073a026*

40. R. Al-Itry, K. Lamnawar, A. Maazouz. Reactive extrusion of PLA, PBAT with a multifunctional epoxide: Physico-chemical and rheological properties. *Eur. Polym. J.* 2014;58:90-102. doi:*https://doi.org/10.1016/j.eurpolymj.2014.06.013*

41. I. Korbag, S. Mohamed Saleh. Studies on the formation of intermolecular interactions and structural characterization of polyvinyl alcohol/lignin film. *Int. J. Environ. Stud.* 2016;73(2):226-235. doi:*https://doi.org/10.1080/00207233.2016.1143700*

42. J. Zhuang, M. Li, Y. Pu, A.J. Ragauskas, C.G. Yoo. Observation of potential contaminants in processed biomass using fourier transform infrared spectroscopy. *Appl. Sci.* 2020;10(12):4345. doi:*https://doi.org/10.3390/app10124345*

43. N. Cachet, S. Camy, B. Benjelloun-Mlayah, J.-S. Condoret, M. Delmas. Esterification of organosolv lignin under supercritical conditions.*Ind. Crops Prod.* 2014;58:287-297. doi:*https://doi.org/10.1016/j.indcrop.2014.03.039*

44. A.S. Rosa, E.A. Disalvo, M. Frias. Water behavior at the phase transition of phospholipid matrixes assessed by FTIR spectroscopy.*J. Phys. Chem. B* . 2020;124(29):6236-6244. doi:*https://doi.org/10.1021/acs.jpcb.0c03719*

45. F. Markowicz, A. Szymańska-Pulikowska. Assessment of the decomposition of oxo-and biodegradable packaging using FTIR spectroscopy. *Materials* . 2021;14(21):6449. doi:*https://doi.org/10.3390/ma14216449*

46. H. Li, C. Xu, G. Ni, J. Lu, Y. Lu, S. Shi, M. Li, Q. Ye. Spectroscopic (FTIR, $^{1}$H NMR) and SEM investigation of physicochemical structure changes of coal subjected to microwave-assisted oxidant stimulation. *Fuel* . 2022;317:123473. doi:*https://doi.org/10.1016/j.fuel.2022.123473*

47. A.K. Zak, W.A. Majid, M.E. Abrishami, R. Yousefi. X-ray analysis of ZnO nanoparticles by Williamson–Hall and size–strain plot methods.*Solid State Sci.* 2011;13(1):251-256. doi:*https://doi.org/10.1016/j.solidstatesciences.2010.11.024*

48. B. Nasiri-Tabrizi. Thermal treatment effect on structural features of mechano-synthesized fluorapatite-titania nanocomposite: A comparative study. *J. Adv. Ceram.* 2014;3(1):31-42. doi:*https://doi.org/10.1007/s40145-014-0090-4*

49. S. Wang, J. Wang, J. Yu, S. Wang. Effect of fatty acids on functional properties of normal wheat and waxy wheat starches: A structural basis. *Food Chem.* 2016;190:285-292. doi:*https://doi.org/10.1016/j.foodchem.2015.05.086*

50. S. Shi, Y. Dong, Q. Li, T. Liu, X. Yu. Morphology, structural, thermal and rheological properties of wheat starch–palmitic acid complexes prepared during steam cooking. *RSC Adv.*2020;10(50):30087-30093. doi:*https://doi.org/10.1039/D0RA05954D*

51. A.R. Hernández, O.C. Contreras, J.C. Acevedo, L.G.N. Moreno. Poly (ε-caprolactone) degradation under acidic and alkaline conditions.*Am. J. Polym. Sci* . 2013;3(4):70-75. doi:*https://doi.org/10.5923/j.ajps.20130304.02*

52. W.H. Hoidy, M.B. Ahmad, E.A.J. Al-Mulla, N.A.B. Ibrahim. Preparation and characterization of polylactic acid/polycaprolactone clay nanocomposites. *J. Appl. Sci.* 2010;10(2):97-106. doi:*https://doi.org/10.3923/jas.2010.97.106*

53. Y.-J. Kim, M.R. Park, M.S. Kim, O.H. Kwon. Polyphenol-loaded polycaprolactone nanofibers for effective growth inhibition of human cancer cells. *Mater. Chem. Phys.* 2012;133(2-3):674-680. doi:*https://doi.org/10.1016/j.matchemphys.2012.01.050*

54. Y. Zhang, J. Liao, X. Fang, F. Bai, K. Qiao, L. Wang. Renewable high-performance polyurethane bioplastics derived from lignin–poly (ε-caprolactone). *ACS Sustainable Chem. Eng.* 2017;5(5):4276-4284. doi:*https://doi.org/10.1021/acssuschemeng.7b00288*

55. J. Bang, J.-H. Kim, S.-W. Park, J. Kim, M. Jung, S. Jung, J.-C. Kim, I.-G. Choi, H.W. Kwak. Effect of chemically modified lignin addition on the physicochemical properties of PCL nanofibers. *Int. J. Biol. Macromol.* 2023;240:124330. doi:*https://doi.org/10.1016/j.ijbiomac.2023.124330*

56. Y. Zhang, Q. Zhao, L. Li, R. Yan, J. Zhang, J. Duan, B. Liu, Z. Sun, M. Zhang, W. Hu. Synthesis of a lignin-based phosphorus-containing flame retardant and its application in polyurethane. *RSC Adv.*2018;8(56):32252-32261. doi:*https://doi.org/10.1039/C8RA05598J*

57. C.E. de Araujo Padilha, C. da Costa Nogueira, S.C.B. Matias, J.D.B. da Costa Filho, D.F. de Santana Souza, J.A. de Oliveira, E.S. dos Santos. Fabrication of hollow polymer microcapsules and removal of emulsified oil from aqueous environment using soda lignin nanoparticles.*Colloids Surf., A* . 2020;603:125260. doi:*https://doi.org/10.1016/j.colsurfa.2020.125260*

58. D.S. Silva, W.M. Facchinatto, D.M. Dos Santos, F.I. Boni, T.A. Valdes, A. Leitão, M.P.D. Gremiao, L.A. Colnago, S.P. Campana-Filho, S.J.L. Ribeiro. N-(2-hydroxy)-propyl-3-trimethylammonium, O-palmitoyl chitosan: Synthesis, physicochemical and biological properties.*Int. J. Biol. Macromol.* 2021;178:558-568. doi:*https://doi.org/10.1016/j.ijbiomac.2021.02.031*

59. M.B. Agustin, K.S. Mikkonen, M. Kemell, P. Lahtinen, M. Lehtonen. Systematic investigation of the adsorption potential of lignin-and cellulose-based nanomaterials towards pharmaceuticals. *Environ. Sci.: Nano* . 2022;9(6):2006-2019. doi:*https://doi.org/10.1039/d2en00186a*

60. Y. Chai, Y. Wang, B. Li, W. Qi, R. Su, Z. He. Microfluidic synthesis of lignin/chitosan nanoparticles for the pH-responsive delivery of anticancer drugs. *Langmuir* . 2021;37(23):7219-7226. doi:*https://doi.org/10.1021/acs.langmuir.1c00778*

61. B. Yang, W. Zeng, Z.H. Peng, S.R. Liu, K. Chen, X.M. Tao. A fully verified theoretical analysis of contact-mode triboelectric nanogenerators as a wearable power source. *Adv. Energy Mater.*2016;6(16):1600505. doi:*https://doi.org/10.1002/aenm.201600505*

62. J. Peng, S.D. Kang, G.J. Snyder. Optimization principles and the figure of merit for triboelectric generators. *Sci. Adv.*2017;3(12):eaap8576. doi:*https://doi.org/10.1126/sciadv.aap8576*

63. S. An, H.S. Jo, G. Li, E. Samuel, S.S. Yoon, A.L. Yarin. Sustainable nanotextured wave energy harvester based on ferroelectric fatigue-free and flexoelectricity-enhanced piezoelectric P (VDF-TrFE) nanofibers with $BaSrTiO_3$ nanoparticles. *Adv. Funct. Mater.*2020;30(25):2001150. doi:*https://doi.org/10.1002/adfm.202001150*

64. Z. Fang, K.H. Chan, X. Lu, C.F. Tan, G.W. Ho. Surface texturing and dielectric property tuning toward boosting of triboelectric nanogenerator performance. *J. Mater. Chem. A* . 2018;6(1):52-57. doi:*https://doi.org/10.1039/C7TA07696G*

65. X.-S. Zhang, J. Brugger, B. Kim. A silk-fibroin-based transparent triboelectric generator suitable for autonomous sensor network.*Nano Energy* . 2016;20:37-47. doi:*https://doi.org/10.1016/j.nanoen.2015.11.036*

66. H.J. Kim, J.H. Kim, K.W. Jun, J.H. Kim, W.C. Seung, O.H. Kwon, J.Y. Park, S.W. Kim, I.K. Oh. Silk nanofiber-networked bio-triboelectric generator: silk bio-TEG. *Adv. Energy Mater.* 2016;6(8):1502329. doi:*https://doi.org/10.1002/aenm.201502329*

67. H.-J. Kim, E.-C. Yim, J.-H. Kim, S.-J. Kim, J.-Y. Park, I.-K. Oh. Bacterial nano-cellulose triboelectric nanogenerator. *Nano Energy* . 2017;33:130-137. doi:*https://doi.org/10.1016/j.nanoen.2017.01.035*

68. R. Ccorahua, J. Huaroto, C. Luyo, M. Quintana, E.A. Vela. Enhanced-performance bio-triboelectric nanogenerator based on starch polymer electrolyte obtained by a cleanroom-free processing method.*Nano Energy* . 2019;59:610-618. doi:*https://doi.org/10.1016/j.nanoen.2019.03.018*

69. Y. Lu, X. Li, J. Ping, J.s. He, J. Wu. A flexible, recyclable, and high-performance pullulan-based triboelectric nanogenerator (TENG).*Adv. Mater. Technol.* 2020;5(2):1900905. doi:*https://doi.org/10.1002/admt.201900905*

70. K. Yan, X. Li, X.-X. Wang, M. Yu, Z. Fan, S. Ramakrishna, H. Hu, Y.-Z. Long. A non-toxic triboelectric nanogenerator for baby care applications. *J. Mater. Chem. A* . 2020;8(43):22745-22753. doi:*https://doi.org/10.1039/d0ta08909e*

71. Z. Yu, Y. Wang, J. Zheng, Y. Xiang, P. Zhao, J. Cui, H. Zhou, D. Li. Rapidly fabricated triboelectric nanogenerator employing insoluble and infusible biomass materials by fused deposition modeling. *Nano Energy* . 2020;68doi:*https://doi.org/10.1016/j.nanoen.2019.104382*

72. D. Park, J.-H. Hong, D. Choi, D. Kim, W.H. Jung, S.S. Yoon, K.H. Kim, S.J.N.E. An. Biocompatible and mechanically-reinforced tribopositive nanofiber mat for wearable and antifungal human kinetic-energy harvester based on wood-derived natural product.*Nano Energy* . 2022;96:107091. doi:*https://doi.org/10.1016/j.nanoen.2022.107091*

**Table 1.** $M_{\mathrm{w}}$ of kraft, hydrophilic, and hydrophobic lignins.

| **Lignin** | $M_{\mathbf{w}}$ **(Da)** |
|---|---|
| Kraft lignin | 4,826 |
| Hydrophilic lignin | 6,654[a] |
| Hydrophobic lignin | 13,430 |

[a]Determined by elemental analysis and the degree of substitution due to the insolubility of hydrophilic lignin in the mobile phase (*i.e.* , tetrahydrofuran) of GPC.

**Table 2.** Comparison of materials, methods, and performances of the previously-reported tribopositive biomaterial-based TENGs.

| **Cases in Fig. 4f** | **Year** | **Tribopositive bio-material** | **Tribonegative material** | **Type** | **Fabrication method** | **External force Type** | **External force Applied force [N]** | **External force Applied frequency [Hz]** | **Maximum output voltage [V]** | **Efficiency V N$^{-1}$** | **Efficiency V m$^{-2}$** | **Efficiency V N$^{-1}$ m$^{-2}$** | **Cyc** |
|---|---|---|---|---|---|---|---|---|---|---|---|---|---|

| Cases in Fig. 4f | Year | Tribopositive biomaterial | Tribonegative material | Type | Fabrication method | External force | External force | External force | Maximum output voltage [V] | Efficiency | Efficiency | Efficiency | Cyc |
|---|---|---|---|---|---|---|---|---|---|---|---|---|---|
| a | 2016 | Silk | Polyethylene terephthalate (PET) | Film | Coating | Tapping | - | - | 40 | - | 50,000 | - | 18,00 |
| b | 2016 | Silk | Polymide (PI) | Film | Electrospinning | Tapping | 44.5 | 10 | 26 | 0.58 | 9,290 | 209 | 25,00 |
| c | 2017 | Cu | Bacterial nanocellulose from *Acetobacter xylinum* | Film | Casting | Tapping | 51.2 | 10 | 23 | 0.45 | 9,200 | 180 | - |
| d | 2018 | Soy protein | Polyimide (PI) | Film | Solution blowing | Tapping | 21.5 | 10 | 5 | 0.23 | 5,710 | 266 | 96,00 |
| e | 2019 | Starch from potato | Polytetrafluoroethylene (Teflon) | Film | Casting | Tapping | 10 | 8 | 2 | 0.3 | 5,000 | 500 | - |
| f | 2019 | Pullulan | Polyimide (PI) | Film | Casting | Tapping | - | 10 | 79 | - | 12,340 | - | - |
| g | 2020 | Carboxymethyl cellulose sodium | Carboxymethyl chitosan | Film | Electrospinning | Tapping | - | 2 | 3 | - | 3,330 | - | 3000 |
| h | 2020 | Polyamide (PA)/Lignin | Polydimethylsiloxane (PDMS), Polyethylene (PE) | Film | Fused deposition modeling | Tapping | 100 | 30 | 308 | 3.08 | 25,700 | 256 | - |
| i | 2022 | *Ulmus davidiana* var. *japonica* root bark/PCL | Polytetrafluoroethylene (Teflon) | Film | Electrospinning | Tapping | 20 | 8 | 80 | 4 | 32,000 | 1,600 | 100,0 |

| Cases in Fig. 4f | Year | Tribopositive bio-material | Tribonegative material | Type | Fabrication method | External force | External force | External force | Maximum output voltage [V] | Efficiency | Efficiency | Efficiency | Cyc |
|---|---|---|---|---|---|---|---|---|---|---|---|---|---|
| j | 2022 | Sulfonated lignin/Polyvinyl alcohol (PVA) | Polytetrafluoroethylene (Teflon) | Film | Electrospinning | Tapping | 40 | 10 | 116 | 2.9 | 72,500 | 1,812.5 | |
| | 2023 | Lignin/PCL | Polytetrafluoroethylene (Teflon) | Film | Electrospinning | Tapping | 9 | 9 | 93 | 10.33 | 37,200 | 4133.33 | |

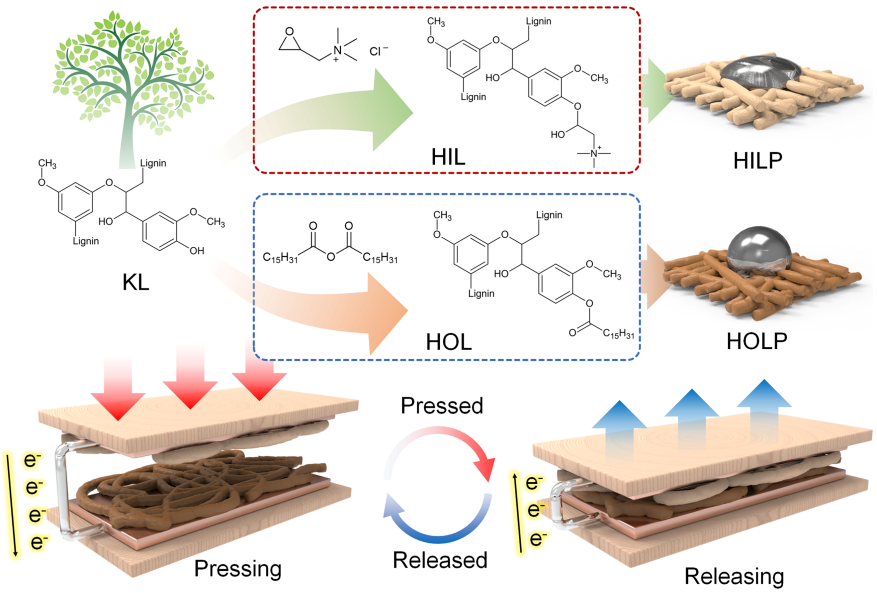


**Figure 1.** Schematic of the process employed to transform KL into HIL and HOL and the operating mechanism of LP-TENG as an energy harvester.

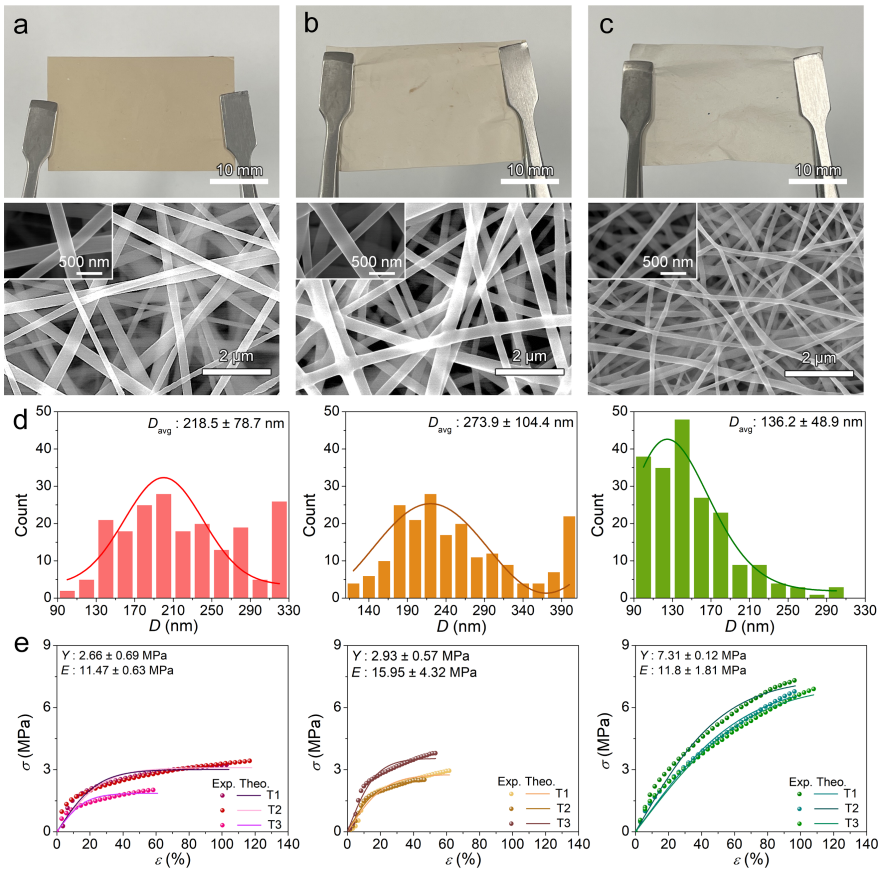


**Figure 2.** Photos and SEM images of electrospun NF mats of (a) KLP, (b) HILP, and (c) HOLP cases. (d) Fiber size distributions and (e) stress-strain curves for KLP, HILP, and HOLP NF mats.

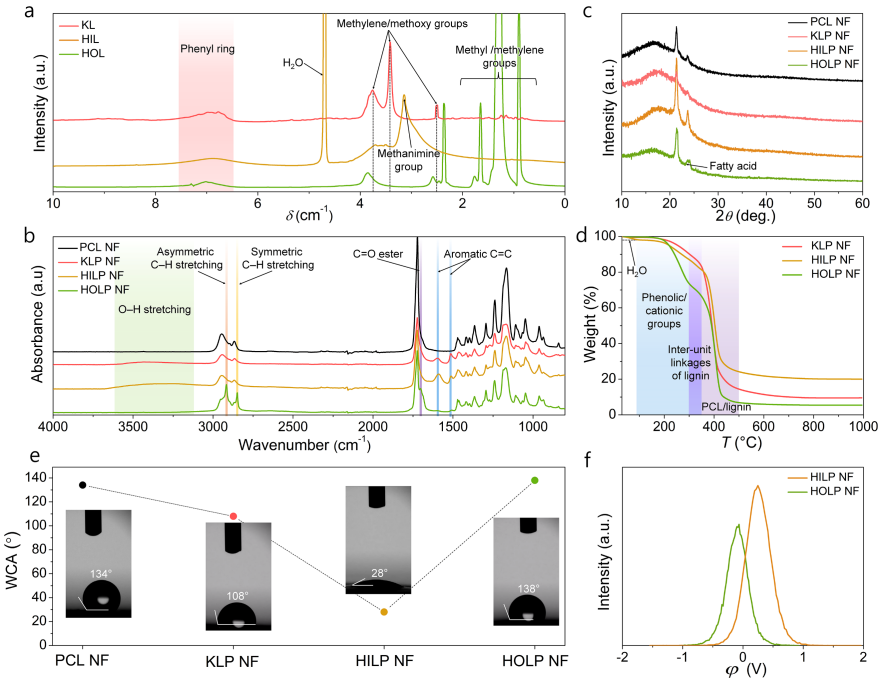


**Figure 3.** (a) $^1$H NMR spectra of KL, HIL, and HOP powders. (b) FTIR spectra and (c) XRD patterns of PCL, KLP, HILP, and HOLP NF mats. (d) TG curves and (e) water contact angles of KLP, HILP, and HOLP NF mats. (f) Surface potential ($\varphi$ ) of HILP and HOLP NF mats.

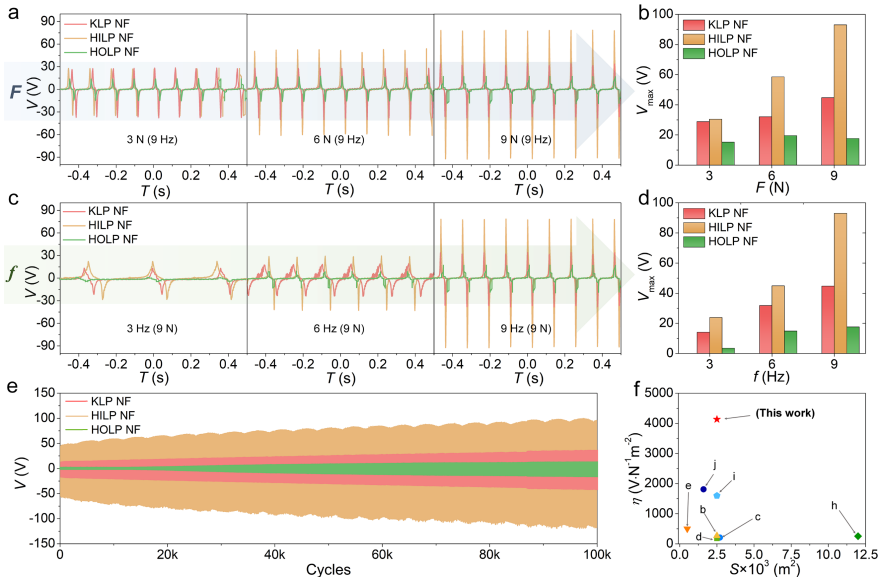


**Figure 4.** $V$ signals of the KLP, HILP, and HOLP-TENGs with (a, b) varying $F$ from 3 to 9 N with a fixed $f$ of 9 Hz and (c, d) varying $f$ from 3 to 9 Hz with a fixed $F$ of 9 N. (e) Cyclic tapping tests of the KLP-, HILP-, and HOLP-TENGs for 100,000 cycles. (f) $\eta$ *vs* . $S$ for the previously-reported tribopositive biopolymer-based TENGs.

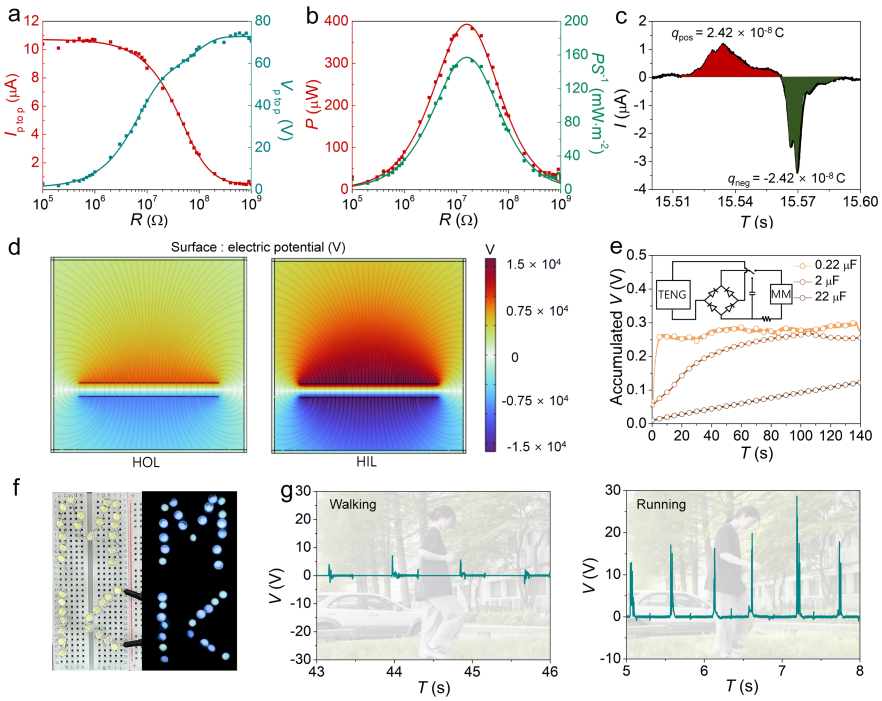


**Figure 5.** (a) $V_{\text{ptop}}$ and $I_{\text{ptop}}$ as a function of $R$ ranging from $10^5$ to $10^9$ Ω and (b) the corresponding $P$ and $PS^{-1}$. (c) A short-circuit $I$ signal of HILP-TENG for electric charge measurement. (d) Simulation results obtained using COMSOL. (e) Accumulated $V$ signals for different capacitors. (f) LED operation using the HILP-TENG. (g) $V$ signals obtained from the HILP-HOLP-TENG during walking and running.